Friction **12**(3): 522–538 (2024)
https://doi.org/10.1007/s40544-023-0790-2
ISSN 2223-7690
CN 10-1237/TH
RESEARCH ARTICLE

High-temperature tribological performance of functionally graded Stellite 6/WC metal matrix composite coatings manufactured by laser-directed energy deposition

Marta OSTOLAZA[1*], Alaitz ZABALA[2], Jon Iñaki ARRIZUBIETA[1], Iñigo LLAVORI[2], Nagore OTEGI[2], Aitzol LAMIKIZ[1]

[1] *Department of Mechanical Engineering, University of the Basque Country UPV/EHU, Plaza Torres Quevedo 1, Bilbo 48013, Spain*

[2] *Faculty of Engineering, Mechanics and Industrial Production, Mondragon Unibertsitatea, Loramendi 4, Mondragon 20500, Spain*

Received: 21 December 2022 / Revised: 17 March 2023 / Accepted: 19 June 2023

Abstract: Wear-driven tool failure is one of the main hurdles in the industry. This issue can be addressed through surface coating with ceramic-reinforced metal matrix composites. However, the maximum ceramic content is limited by cracking. In this work, the tribological behaviour of the functionally graded WC-ceramic-particle-reinforced Stellite 6 coatings is studied. To that end, the wear resistance at room temperature and 400 °C is investigated. Moreover, the tribological analysis is supported by crack sensitivity and hardness evaluation, which is of utmost importance in the processing of composite materials with ceramic-particle-reinforcement. Results indicate that functionally graded materials can be employed to increase the maximum admissible WC content, hence improving the tribological behaviour, most notably at high temperatures. Additionally, a shift from abrasive to oxidative wear is observed in high-temperature wear testing.

Keywords: friction, coating, metal matrix composite, functionally graded materials, high temperature, laser-directed energy deposition

1 Introduction

It is well known that the pace of the automotive industry is strongly set by governmental restrictions concerning environmental issues. In terms of emissions, the European Commission set a 95 g CO_2/km target level for 2021, while 15% and 37.5% reduction goals were established for 2025 and 2030, respectively [1]. Vehicle manufacturers agree that lightening is a critical factor for attaining energy-efficient cars, regardless of the propulsion technology [2]. The most promising solution for minimising CO_2 emissions, whilst increasing the safety and improving the crash performance of vehicles, relies on the implementation of modern advanced high-strength steels (AHSS) as they enable the reduction of the weight of automotive components [3]. Unfortunately, these materials present low room temperature formability and high spring back [4]. Therefore, temperature-assisted processes, i.e., hot stamping or press hardening, are necessary to form AHSS components [5].

In hot stamping processes, the tool damage caused by wear and friction during the high-temperature forming process is a hindrance in terms of productivity and tool lifetime [4], and stems from the unavoidable contact between the tool and the processed blanks [6]. Unfortunately, conventional lubricants cannot be employed to counter these phenomena, as the temperature range of the manufacturing process is far outside the working range of most lubricants [7].

Friction problems in hot forming tools can be overcome by surface treatments and deposition of advanced coatings [8, 9]. At this point, the localised heat input and the rapid solidification of materials

* Corresponding author: Marta OSTOLAZA, E-mail: marta.ostolaza@ehu.eus

inherent to laser processing, place laser-directed energy deposition (L-DED) in an advantageous position compared to traditional coating technologies [10]. Indeed, L-DED yields minimum substrate affection and low distortion, but high integrity coatings [11]. Consequently, demanding geometrical tolerances can be met, while providing a good bond between substrate and coating. Furthermore, the typically complex surfaces of tooling are not restrictive for L-DED owing to its freeform ability.

In surface engineering, metallic and non-metallic materials are often used to improve the wear resistance of steel substrates. Alloying with elements such as niobium, vanadium, or tungsten, has been demonstrated to extend the lifetime of H13 tool steel [12]. The deposition of complex alloys such as FeCrMoVC onto tool steel substrates has been investigated too [13]. Moreover, wear-resistant high entropy alloy (HEA) coatings have been tested in real process conditions and promising results have been obtained [14]. On the other hand, Co-base wear-resistant alloys, such as Stellite 6, possess high wear resistance not only at room temperature but also when subject to high temperatures [15, 16]. The solid-solution of carbide-forming elements and the precipitation hardening are responsible for the improved mechanical properties of such alloys [17]. In addition, the good tribological performance at high temperatures is due to the formation of an oxide layer, which acts as a lubricant and mitigates friction [18]. Finally, surface engineers often resort to ceramics and ceramic hard metal coatings to further increase the resistance to wear due to their high hardness [6]. In this regard, laser processing technologies enable a localised dispersion of ceramic particles [4] or the deposition of ceramic particle-reinforced metal matrix composite (MMC) coatings [19].

The enhanced tribological performance of WC-reinforced MMCs has been extensively reported in the literature. Nurminen et al. investigated the abrasion resistance of different matrix and reinforcement materials [20]. They concluded that spherical WC reinforcement resulted in the best tribological performance. Bartkowski and Kinal found that the wear resistance of the Stellite 6 Co-base alloy increases when embedding WC ceramic particles [21]. They concluded that when the volumetric fraction of WC is too high or the hardness of the matrix is too low, a more intensive wear mechanism of the coatings is promoted. Nonetheless, in general terms, an enhancement of the surface properties of the base material was attained. Later, when applying the developed coating to a real industrial case study in the field of agriculture, they obtained a 25% increase in the durability of tooling [22]. Also, Ni-base and Co-base matrixes are of particular interest when high-temperature wear performance is targeted [23]. Hence, more recent works have focused on characterising the high-temperature tribological behaviour of these coatings. Erfanmanesh et al. investigated the high-temperature performance of WC-Co and Ni/WC-Co coatings in terms of wear [24]. They obtained a substantial improvement in the wear resistance and they concluded that soft abrasive and adhesive wear were dominant. Wang et al. also focused on high-temperature wear testing and confirmed the good behaviour of Stellite 6/WC coatings [25]. In addition, an improvement in the wear resistance of the coatings following the WC content was demonstrated. However, coatings with >20 wt% of WC showed a significant drop in terms of thermal fatigue. Lastly, Karmakar et al. investigated the high-temperature abrasive wear of AISI H13 tool steel coated with Stellite 6 and Stellite 6/WC [26]. Composite coatings showed a higher abrasion resistance in the range of temperatures up to 650 °C, as compared to the base material. The improvement was more evident the higher the temperature of the wear test.

In terms of L-DED of MMCs, the production of good quality coatings is still a challenge. For instance, material incompatibility is an issue to tackle [27]. Defects related to metallurgical integrity (pores or cracking) are frequently encountered [28]. As a response, multiple methods have been proposed to eliminate cracking, namely, substrate preheating, the addition of rare earth oxides, or the elimination of the sharp transition between substrates and coatings through functionally graded materials (FGM) [19]. The FGM strategy is particularly interesting for the L-DED technology [27]. In fact, the composition of

the feedstock in the production of multi-material structures can be easily controlled. In the case of MMCs, a layer-wise variation of the volumetric fraction of the reinforcement is readily attainable. Typically, functionally graded materials exhibit lower residual stresses, which are the main cause of cracking in MMCs. Hence, the FGM strategy can be implemented to improve the integrity of MMC coatings produced by L-DED. In fact, Xu et al. reported that the crack sensitivity of MMC consisting of Stellite 6 and WC was significantly reduced when introducing functionally graded transitions as compared to sharp material transitions [29]. In addition, they studied the room-temperature wear resistance of mono-compositional and functionally graded MMCs and got similar results. Nonetheless, to the authors' knowledge, the high-temperature wear performance of functionally graded MMC coatings as compared to mono-compositional MMC coatings has not been studied so far.

Motivated by the research gap identified in the literature, in the present work, the high-temperature wear performance of functionally graded MMCs is investigated. Indeed, the FGM strategy can be used to increase the admissible WC% in MMC coatings, with subsequent performance improvement. The enhancement of the wear properties of the coated and uncoated samples at both room and high temperatures is assessed. Furthermore, the performance of functionally graded and mono-compositional coatings is compared. Lastly, the most relevant wear mechanisms for each scenario and material are identified. The main contributions of the present research work are as follows.

1) The crack sensitivity of multilayer MMC coatings deposited with different strategies (i.e., FGM and mono-composition) is assessed.

2) The wear resistance of L-DED coatings is evaluated both at room temperature and 400 °C. Coatings with different top layer compositions and manufactured with graded and not graded strategies are studied. All results are compared to the uncoated reference specimens.

3) The microstructural evolution of the matrix when varying the composition of the feedstock is studied. Moreover, the hardness of the matrix and the surface hardness of the produced specimens are investigated.

2 Materials and methods

2.1 Materials

In this research, AISI H13 tool steel was selected as the substrate material. The dimensions of the substrate billets are 45 mm × 35 mm × 8 mm. This material is frequently employed in the die and mould industry for high-temperature process tooling. The surface coatings applied to the AISI H13 consist of a Co-base matrix, similar to Stellite® 6, and a WC reinforcement. Commercial L-DED powders are employed for coating production, namely, MetcoClad 6 and MetcoClad 52001 (Oerlikon Metco). The granulometry of both powders is in the range of 45 to 106 μm. The composition of the substrate material and the L-DED feedstock is shown in Table 1.

2.2 Test specimen preparation: L-DED process and heat treatment of reference specimens

The coating specimens were produced by means of a TruLaser Cell 3000 L-DED machine. The laser source is a 3 kW Yb:YAG disk laser, with a 1,030 nm wavelength. The laser spot diameter at the focal plane was set at 1.75 mm. To enable an adequate process parameter selection, different sets of parameters with varying power, feed rate, and mass flow rate were tested before choosing the optimal ones. To that end, single-clad experiments were carried out. The processing conditions tested are shown in Table 2.

Table 1 Composition of the materials employed wt% [30–32].

Material	Co	Cr	W	Fe	Ni	Si	C	Mo	Mn	P	S	V
MetcoClad 6	Bal.	28.0	4.0	3.0	3.0	1.5	1.0	1.0	0.0	0.0	0.0	0.0
MetcoClad 52001	0.0	0.0	Bal.	0.19	0.0	0.0	4.03	0.0	0.0	0.0	0.0	0.0
AISI H13	0.0	5.13	0.0	Bal.	0.0	1.03	0.39	1.43	0.4	0.03	0.03	1.0

Table 2 Single-clad experimental tests to select optimal process parameters.

Test	Power (W)	Feed rate (mm/min)	Mass flow rate (g/min)
1	700	400	2.97
2	600	400	2.97
3	800	400	2.97
4	700	450	3.34
5	700	350	2.60

Once the best process parameters were selected, different overlapping conditions were tested, namely 30% and 40%.

Most promising results were obtained for the first set of parameters and 30% overlap. Indeed, such processing conditions resulted in defect-free clads soundly bonded to the substrate. In Fig. 1, the selected single-clad, single-layer, and multi-layer tests are shown.

The L-DED parameters were kept constant for all experiments, at 700 W laser power and 400 mm/min feed rate. In addition, the volumetric rate of the feedstock was fixed at 0.35 cm^3/min, which results in a constant clad geometry (0.38 mm height and 1.84 mm width). Thus, the mass flows of the matrix and the reinforcement material were calculated for each layer according to the target composition and the density of the material. The powder is fed through a GTV PF 2/2 disk feeder, which comprises two independent hoppers. In this manner, the powder flow of each one of the hoppers can be tuned independently and, therefore, the composition of the powder mixture is controlled precisely. The powder flows provided by each hopper are combined in a mixing chamber and fed to the melt pool through a discrete coaxial nozzle. Argon at a rate of 12 L/min and helium at a rate of 4 L/m were used as shielding and carrier gases, respectively. As far as the deposition strategy is concerned, a zig path (one-way deposition strategy) was followed in each layer, alternating the X and Y deposition directions layer upon layer.

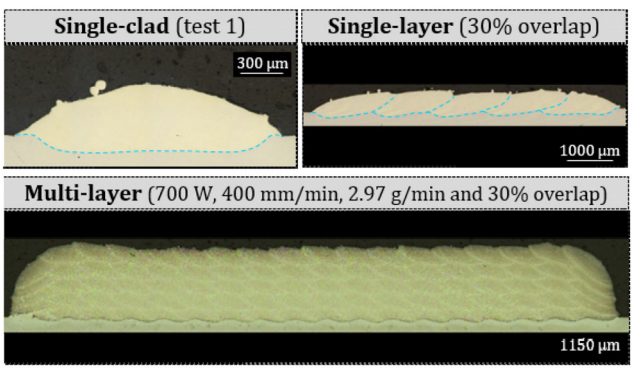

Fig. 1 Single-clad, single-layer, and multi-layer samples produced with the optimal processing conditions.

The dimensions of the deposited coatings are roughly 10 mm×25 mm×2 mm. Four different coating designs were tested and each specimen was constituted by four layers (Fig. 2), whose composition varies according to Table 3. In total, four specimens were produced for each coating design, one for metallurgical and matrix hardness characterisation and three for wear testing and surface hardness measurements. In addition, uncoated AISI H13 samples were also prepared for wear testing and surface hardness measurement. To that end, three AISI H13 specimens were ground and heat-treated, by quenching and tempering in accordance with Fig. 3.

2.3 Inspection of the metallurgical integrity and microstructural analysis of the samples

The Nikon Optiphot-100 optical microscope was employed for microstructural analysis purposes. To

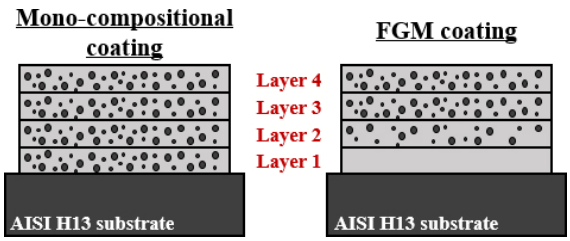

Fig. 2 Layer disposition in mono-compositional and FGM specimens.

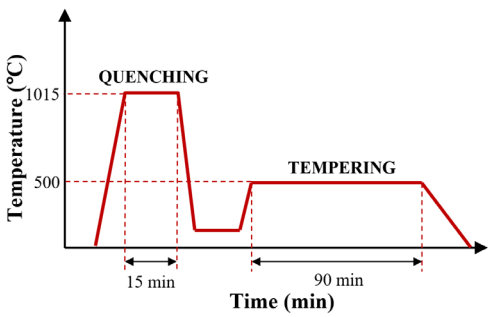

Fig. 3 Q+T heat treatment of the reference uncoated AISI H13 specimens.

Table 3 Layer composition of L-DED specimens (MC6 and MC52001 stand for MetcoClad 6 and MetcoClad 52001, respectively).

Layer	Stellite 6 Mono	5% WC Mono	5% WC FGM	10% WC FGM
1	100% MC6	95% MC6 5% MC52001	100% MC6	100% MC6
2	100% MC6	95% MC6 5% MC52001	97.5% MC6 2.5% MC52001	95% MC6 + 5% MC52001
3	100% MC6	95% MC6 5% MC52001	95% MC6 5% MC52001	90% MC6 + 10% MC52001
4	100% MC6	95% MC6 5% MC52001	95% MC6 + 5% MC52001	90% MC6 + 10% MC52001

that end, two cross-sectional samples were extracted from the first specimen of each coating design by means of wire-Electro Discharge Machining (w-EDM). The samples were subsequently mounted, ground, and polished following the appropriate metallographic procedure. Lastly, the microstructure was revealed by electrolytic etching with 10% oxalic acid solution at 10 V and 1 A for 1–3 s.

In addition, the surface integrity of the three remaining specimens was inspected by means of the Leica Z6 AP0 optical microscope right before tribological characterisation. With the aim of developing processing maps for the production of MMC coatings based on the criterion of surface integrity, the surface cracking of the manufactured samples was quantified with regard to three parameters, i.e., the number of cracked samples (out of 3), the number of cracks, and the average width of the cracks. The resolution of the equipment employed for this inspection was 351 LP/mm, that is, about 3 μm. Lastly, with the intent of increasing the reliability of these measurements, the width of cracks was measured ten times per sample. The ultimate objective of these processing maps is to determine the maximum admissible WC content in MMC coatings, depending on the L-DED strategy employed in their production.

2.4 Characterisation of the hardness of the matrix and the surface hardness of the coating

As far as the mechanical characterisation is concerned, both the hardness of the matrix and the hardness of the coating were measured. For the first one, the cross-sectional samples were employed, as indicated in Fig. 4. The Future-Tech FM-800 microhardness tester was employed for the matrix characterisation. Indentations with 300 gf and 12 s dwell time following the scheme in Fig. 4 were carried out. In each line, 13 indentations were done with a 500 μm distance between centres.

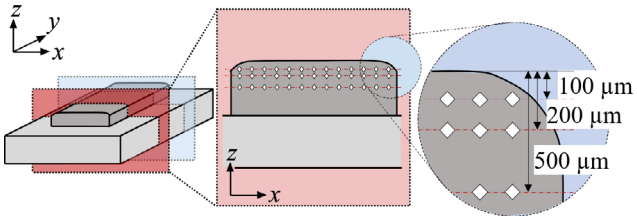

Fig. 4 Position of the indentations for the microhardness characterisation. Measurements at different distances from the surface are indicated by the red lines.

On the contrary, the hardness of the coating was measured at the surface of the samples using a Computest SC Ernst macrohardness tester before step 6 of Fig. 5. This tester follows the Rockwell C principle and five indentations were done for each coating design.

2.5 Tribological characterisation of the coatings

The specimen preparation procedure for tribological testing is shown in Fig. 5. A pocket in the substrate material was milled and then coated following the parameters specified in Section 2.2. The flatness of the sample was ensured by means of w-EDM of the coated surface and backside grinding. Then, the top surface of the coatings to be studied was manually polished with a SiC abrasive paper until a surface roughness of Ra 0.70±0.07 μm, Rz 5.00±0.70 μm, was reached, note that the initial Ra and Rz were 3.18±0.25 μm and 19.94±1.60 μm, respectively. This was done before the tribological characterisation. Lastly, the parameters of the tribological testing were selected to ensure an adequate representation of real hot stamping conditions.

The process parameters during sheet metal forming can be quite broad. After analysing several component simulations, Cillaurren et al. observed that the contact pressure on flat areas ranges between 3–15 MPa on average, while it rises to 20–100 MPa for curved areas, with maximum values up to 200 MPa.

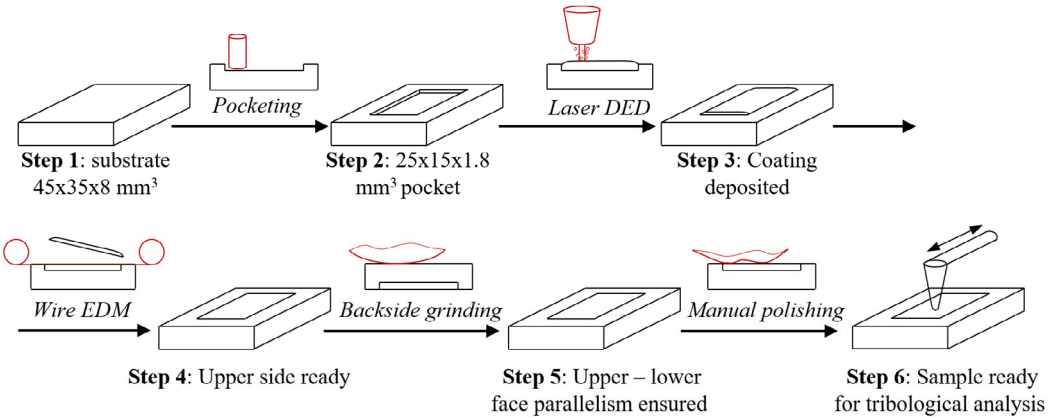

Fig. 5 Scheme of the sample preparation process followed for reciprocating wear testing.

Similarly, the sliding velocities of the inner areas ranged between 20–25 mm/s on average, whilst the outer areas raised to 50 mm/s, with maximum values reaching up to 200 mm/s [33]. When considering temperature ranges, it is important to pay attention to the maximum temperature that hot-forming tools typically withstand. Hoffman and Steinbeiss observed a cyclic evolution of tool temperature in hot stamping processes and reached a stable cycle emerging after about 10 cycles. For the case they presented, the maximum temperature reached was around 375 °C [34]. Considering that the temperature of the tooling strongly depends on the cooling system design [35], for this study, a temperature of 400 °C has been chosen to represent the severe end of the spectrum of hot stamping processes. In order to obtain a comparative range of wear resistance and friction behaviour of the newly developed functionally graded Stellite 6/WC metal matrix composite coatings, an accelerated test under standardised ball-on-flat linear reciprocating sliding configuration [36] against a reference ceramic counterpart was performed. Tribological test parameter selection was also supported by Wang et al. [25], where Stellite-6/WC coatings produced by laser cladding were tested for the tooling industry. Tests were carried out on the Bruker UMT tribometer, using a 6 mm Ø Si3N4 ball as the counterpart with a normal load of 8 N, which corresponded to 900 MPa average Hertzian contact pressure. Using a 2.5 mm stroke and a reciprocating frequency of 20 Hz, tests were conducted at an average of 100 mm/s linear speed until completing 18,000 cycles (15 min), both at room temperature (RT) and 400 °C. The room temperature experiments were performed under 22±1 °C temperature and 48%±4% relative humidity. The pin and the plate were ultrasonically cleaned in acetone for 10 min followed by air-drying before each test. Three replicates per condition were carried out for good statistical representation

The coefficient of friction was computed through the energy dissipation method under the ASTM G203 standard [37]. Note that average friction coefficient values were computed considering the last 75% of the friction curve to account solely for the steady state friction behaviour, after the running in. Equation (1) shows the formulation of the energy coefficient of friction (ECoF), being E_d the dissipated energy over a cycle, δ^* the slip amplitude, and P the contact load [38].

$$\mu_E = \frac{E_d}{4P\delta^*} \tag{1}$$

A non-contact 3D optical profiler (Sensofar S-Neox, white light interferometry technique) was used with an objective of 20xDI (optical resolution = 0.41 μm, vertical resolution 1 nm) in order to measure the wear scars. Wear scar volume was computed on the areal measurements [39] and 2D profiles were also extracted to characterise the wear scar width and depth in SensoMap Premium 7 software. Lastly, worn surfaces were analysed by scanning electron microscopy (SEM) and energy dispersive spectrometry (EDX).

3 Results

3.1 Cracking sensitivity of MMC coatings produced by L-DED

Surface cracking is a major problem in the L-DED of ceramic-reinforced MMCs. Thus, the maximum tungsten carbide content of MMC coatings is limited by the cracking sensitivity of the material. Figure 6 shows the surface quality of the specimens prepared for tribological characterisation, where the surface cracks are denoted by white arrows. All three specimens corresponding to monolithic Stellite 6 coatings present good surface integrity and no cracking is observed (Fig. 6(a)). Good quality coatings were obtained also when producing functionally graded coatings with tungsten carbide content varying from 0% to 5% WC (Fig. 6(c)). In contrast, two out of the three mono-compositional specimens with 5% WC experienced surface cracking (Fig. 6(b)). Lastly, severe cracking was observed in all specimens manufactured following the FGM strategy with a 0% to 10% WC content variation (Fig. 6(d)).

The cracking of MMCs deposited by L-DED has been widely studied in Ref. [40]. Cracks in these coatings originate from the high residual stresses generated during the deposition process. As a process based on fusion and rapid solidification of materials, parts manufactured by L-DED withstand high-temperature gradients; thus, high thermal stresses can be produced if no specific care is taken. The embrittlement of the matrix due to the processing conditions is also a factor that severely affects surface integrity. The loss of ductility prevents the metal matrix from absorbing the residual stresses of the manufacturing process. Additionally, the reinforcement particles act as stress concentrators [26], which further exacerbate cracking. Hence, the crack sensitivity of this material is going to limit the production of MMC coatings by L-DED and the development of processing maps is useful to better understand their processability.

Based on the analysis of the integrity of the surfaces performed, the cracking phenomenon is quantified by means of three parameters, namely, the number of samples exhibiting cracking (out of the three prepared specimens), the number of cracks present in each sample, and the width of the cracks. Based on such quantification, a processing map has been developed, for which the acceptance criterion established is the quality assurance based on the surface integrity (Fig. 7). It is concluded the maximum admissible WC content is 5% with the FGM strategy and the employed process parameters, whereas this admissible maximum drops below 5% with no cracking mitigation strategy.

It follows from the obtained results that the FGM strategy is a useful tool to prevent cracking. No defects were observed when manufacturing coatings with a 5% WC content at the top layers with the FGM strategy. However, poor results were attained in the not-graded coatings with the same top layer composition. The elimination of the sharp transition alleviates the residual stresses generated during the deposition of successive layers. Thus, the progressive

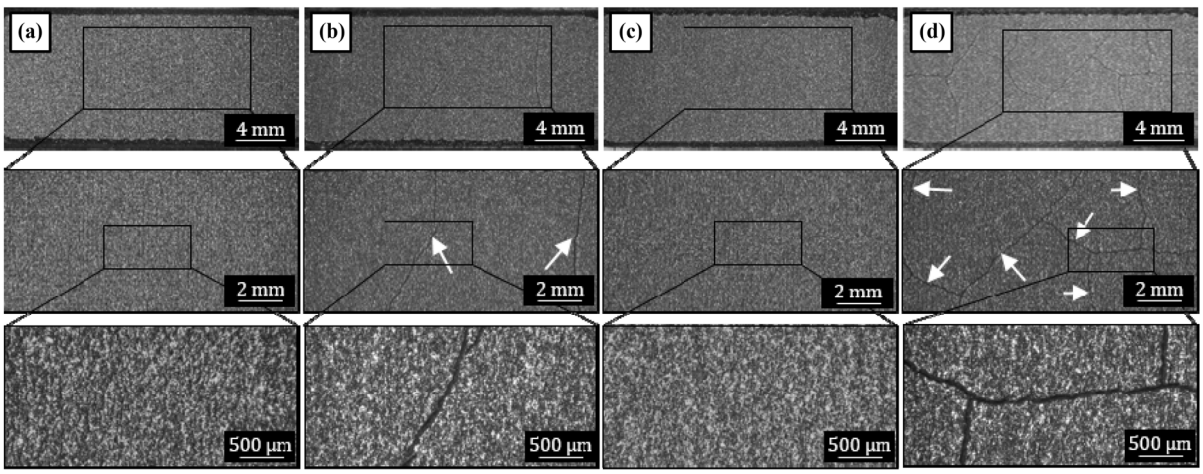

Fig. 6 Surface integrity of produced specimens: (a) Stellite 6 MONO, (b) 5% WC MONO, (c) 5% WC FGM, (d) 10% WC FGM.

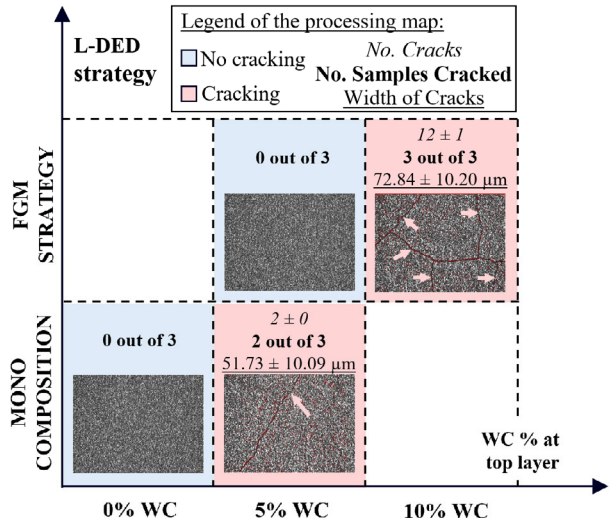

Fig. 7 Processing map for the L-DED of MMC coatings, based on the L-DED strategy and the WC% at the top layer.

variation of the composition used with the FGM strategy reduces the crack sensitivity of ceramic-reinforced MMCs.

3.2 Microstructural characterisation of the MMC coatings

In Fig. 8, the cross-sectional images corresponding to WC-reinforced coatings manufactured with different strategies are shown, namely, 5% WC MONO, 5% WC FGM, and 10% WC FGM. In addition, higher magnification images of regions of interest are provided. In the FGM specimens, the gradual variation of the WC% is clearly evidenced, as no ceramic particles are present in the 1st layer, intermediate WC% is found in the 2nd layer, and the target WC% is reached in the 3rd and 4th layers. Hence, the same volumetric fraction of WC particles is found in the top layer of specimens corresponding to 5% WC FGM and 5% WC MONO, per the design depicted in Table 3.

On the other hand, the heterogeneous distribution of the WC particles is visible in the cross-sectional images of Fig. 8, owing to the Murakami agent employed to etch the tungsten carbide particles selectively. In Fig. 8, the melt pool boundaries and limits of the heat-affected region are depicted to better identify the clads and layers of the coatings. Even in the 5% WC MONO specimen, regions containing a higher volumetric fraction of WC and regions containing a lower fraction are observed. This is a result of the different fluid dynamic behaviour of ceramic and metal particles through the nozzle. Moreover, the heterogeneous distribution of particles is further exacerbated by both gravitational and Marangoni effects in the melt pool.

In terms of metal-ceramic interaction, MMCs manufactured through fusion-based processes often exhibit compositional and microstructural changes in the metal matrix. The thermal nature of fusion-based processes promotes the reaction between the

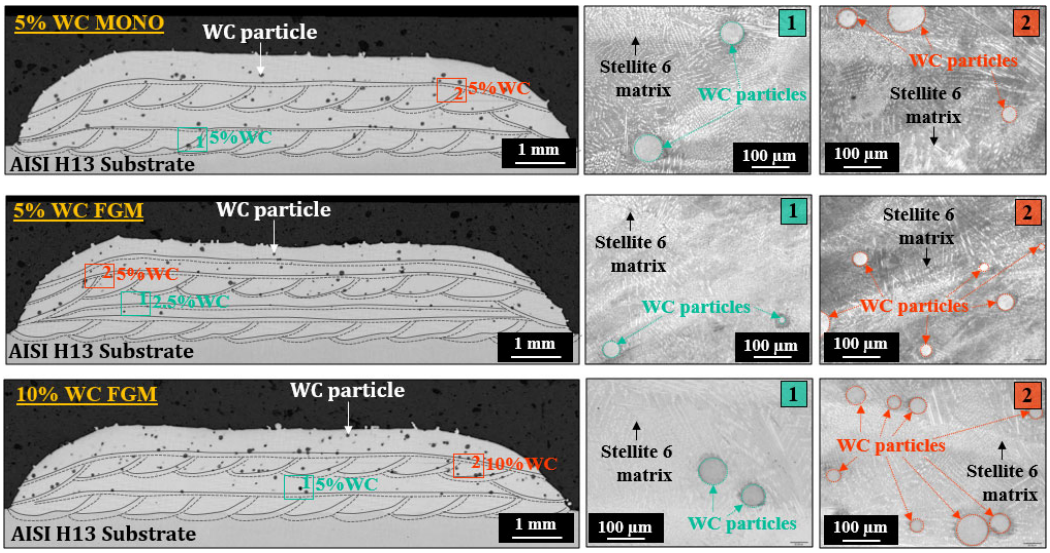

Fig. 8 Cross-sectional images corresponding to WC-reinforced coatings manufactured with mono-composition and functionally graded strategy. Left-hand images etched by Murakami agent (tungsten carbide particles are darkened) and high magnification images are electrolytically etched with 10% oxalic acid.

reinforcement and matrix material. When this interaction is large enough, the matrix is modified globally. However, when little WC concentrations are employed or the exposure time of the material to high temperatures is controlled, this reaction is reduced. Consequently, the matrix is only affected locally and the properties of the base material remain similar from a global perspective. This is the case for the specimens produced in the present study. To validate such a hypothesis, the microstructure of the metal matrix corresponding to the compositions employed throughout the experiments was investigated (Fig. 9).

The base material with no ceramic reinforcement, corresponding to 0% WC (Fig. 9(a)) shows the typical hypoeutectic microstructure of the Stellite 6 Co-base alloy [41]. The white dendrites correspond to the Co-rich γ solution, while the dark phase corresponds to the interdendritic eutectic structure composed of Co-, Cr-, and W-carbides [42]. The same microstructural phases and similar volumetric fractions are observed in all specimens and for all compositions (Figs. 9(b)–9(d)). Slight variations of the grain size are observed, which can be attributed to different cooling rates and solidification speeds, but also to the effect of introducing reinforcement particles. Discrete carbides are a driver for grain refinement [43]. Nonetheless, no clear conclusions can be drawn from this observation, as L-DED clads do have a certain level of microstructural heterogeneity and the observed grain size variations fall within that range. To sum up, no significant modification of the matrix microstructure was observed due to the interaction of the matrix with the reinforcement phase.

3.3 Characterisation of the hardness of the matrix and the surface hardness of the coating

In the present work, the hardness of the MMC coatings is investigated at microscopic and macroscopic scales, to characterise mechanically the matrix and the composite, respectively.

The hardness of the matrix is measured at 100 μm, 200 μm, and 500 μm from the surface of the coating, per Fig. 4. The results corresponding to the matrix hardness characterisation are shown in Fig. 10. Indentations located in or close to WC particles were excluded from the averaging, as the target in this characterisation is the matrix of the MMC coating. Little variation is observed among the specimens studied and all of them show similar hardness values as compared to the reference specimen (i.e., Stellite 6 MONO). Therefore, it is concluded that the effect of the reinforcement particles on the matrix properties is negligible for the employed process parameters and feedstock compositions.

A slightly higher value in the hardness of the matrix of the 10% WC FGM sample is observed in certain profiles. This is ascribed to the reinforcement particles located below the tested surface, which, although not visible, still support the matrix structurally. On the other hand, the 5% WC FGM sample exhibited a slightly lower hardness at a 100 μm distance from the surface. The continuous heating and cooling

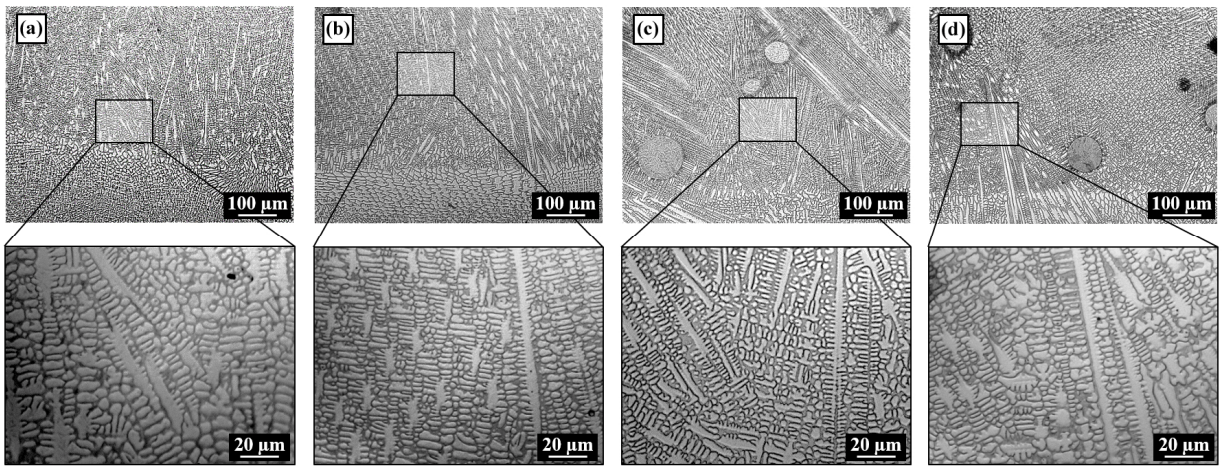

Fig. 9 Microstructural analysis of the MMC specimens: (a) 100% Stellite 6, (b) 97.5% Stellite 6 + 2.5% WC, (c) 95% Stellite 6 + 5% WC, and (d) 90% Stellite 6 + 10% WC.

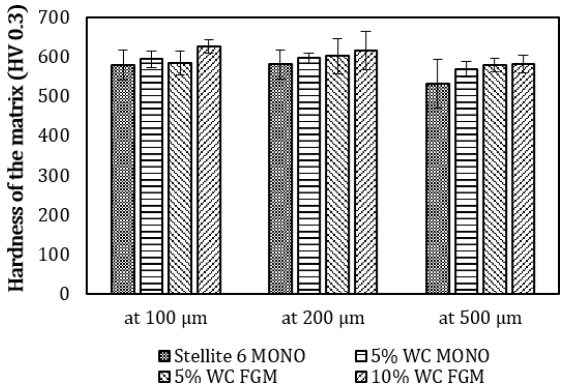

Fig. 10 Hardness of the metal matrix at different distances from the surface. Average values are shown, while error bars indicate the standard deviation.

cycles and subsequent deposition of clads result in heat-affected regions, where the grain size coarsens. This phenomenon is illustrated in Fig. 11. The region tested in the 5% WC FGM corresponds to a heat-affected area, which presents a lower hardness value (on average) in contrast with the region tested in the 10% WC FGM, whose region was not thermally affected by the deposition of additional L-DED clads. In Fig. 11, the indentations are coloured according to the resulting hardness and average values of each profile are also provided (for whose calculation indentations falling on or close to visible tungsten carbide particles were excluded). In addition, higher magnification images of the indentations are included, where the high variability of the HV0.3 test depending on the microstructure of the indented region or the position of the WC particles is demonstrated.

Lastly, the surface hardness of the samples prepared for tribological characterisation is measured. As opposed to matrix characterisation, macroscopic testing methods are adopted. In this manner, the hardness measurements consider the contributions of both phases, i.e., the matrix and the reinforcement. Hence, as shown in Fig. 12, a greater variation among the

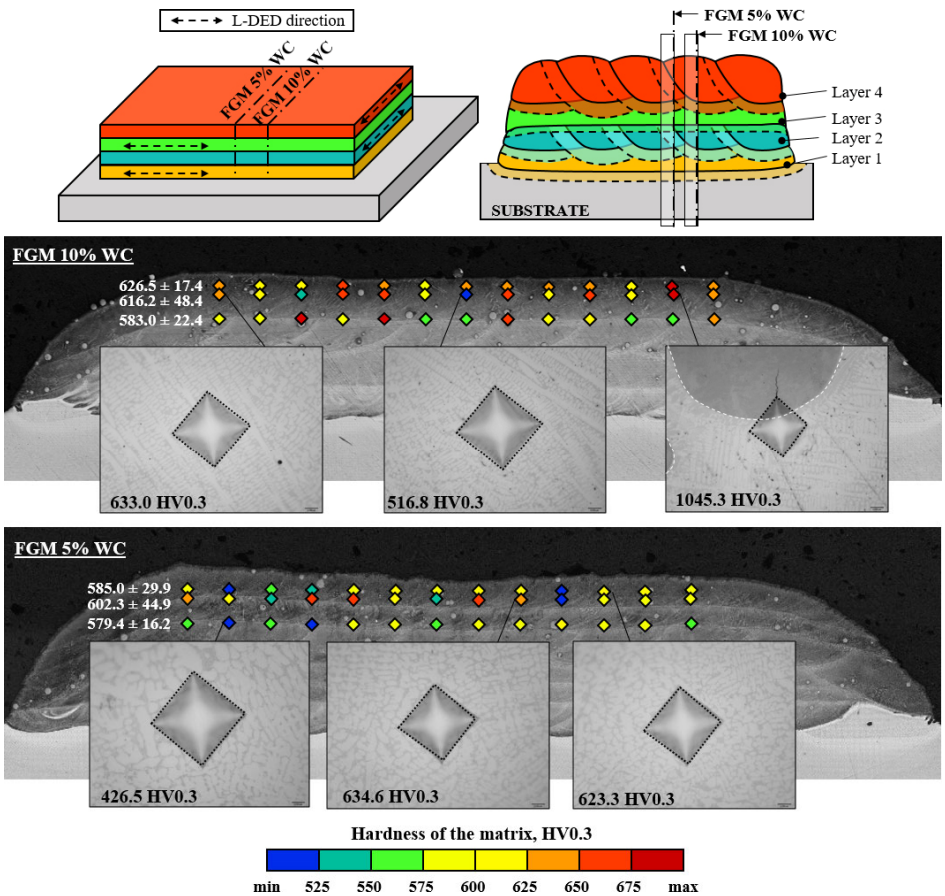

Fig. 11 Schematic illustration of the location of the cross-sectional samples for the characterisation of the hardness. The precise location of the indentations performed is depicted by rhombuses coloured according to the hardness value. Additionally, high-magnification images of representative indentations are shown.

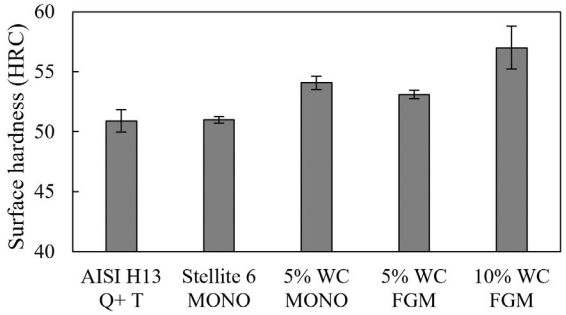

Fig. 12 Surface hardness of the studied specimens. Average results are shown, whilst error bars indicate the standard deviation.

tested coatings is observed. As expected, coatings with a higher volumetric fraction of WC present a higher hardness. The reference material and the coated samples with no reinforcement show similar surface hardness values, roughly 51 HRC. The surface hardness of the samples with 5% WC at the top layer is comparatively higher, between 53 HRC and 54 HRC. In this case, the coatings manufactured with the FGM strategy present a slightly lower surface hardness. This is due to the influence of the layers below, which have a lower content of WC. Indeed, according to ISO 65080:1-2017, the region affected by the HRC measurement is at least 10 times the permanent penetration of the indenter. In the case of a sample having a 55 HRC hardness, this region is 0.9 mm deep, which is thicker than the sum of the thickness of the two upper layers. Therefore, it is logical that the FGM samples exhibit a slightly lower hardness because of the influence of layer 2, which has a lower WC content. Lastly, a substantially higher hardness is observed in the coated samples with 10% WC at the top layer. In fact, a surface hardness as high as 57 ± 1.8 HRC is reported. In these samples, a higher dispersion of the experimental values is observed, most likely due to the uneven distribution of the reinforcement particles shown in Fig. 8 and the lack of integrity of the 10% WC FGM specimens (see Fig. 6).

3.3 Tribological characterisation of the surface coatings

In the room temperature reciprocating tests, coated samples present a lower wear resistance as compared to the uncoated AISI H13 heat-treated substrate (Fig. 13(a)). The quenched and tempered AISI H13 specimens experienced a very low volume loss, owing to the high metallurgical integrity and microstructural features of the hot-rolled substrates (Fig. 12). This good tribological performance is also a result of the carbide formation, martensitic transformation, and grain refinement obtained during the heat treatment. As far as the coated specimens are concerned, a substantial improvement in the wear resistance of WC-reinforced coatings as compared to the monolithic Stellite 6 coatings was observed. Lower volume loss and lower friction coefficients were attained when embedding a ceramic reinforcement into the metal matrix, as shown in Fig. 14, where the friction curves corresponding to both room temperature and high temperature tests are depicted.

Conversely, promising results were obtained in the coated specimens with regard to the high-temperature wear behaviour. As shown in Fig. 13(b), a significant decrease in the volume loss was observed as compared to the uncoated AISI H13 heat-treated reference specimens. The benefit of the surface coatings in terms of high-temperature tribological behaviour is clearly illustrated by the depth and width reduction of the scars (see Fig. 15(b)).

The obtained results at RT and 400 °C suggest that

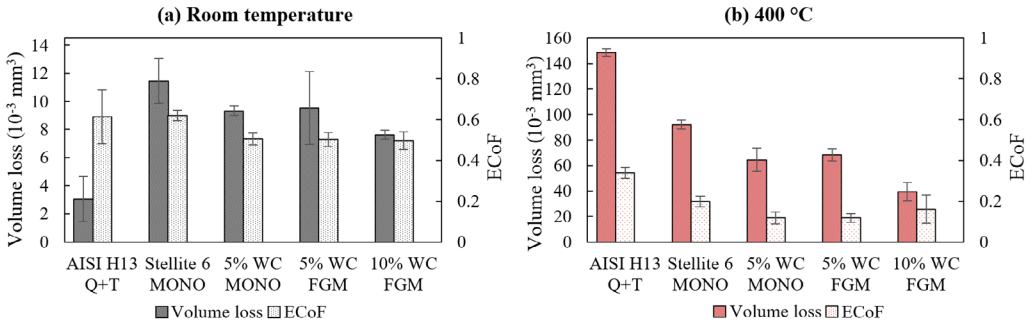

Fig. 13 Volume loss and energy friction coefficient (ECoF) corresponding to the reciprocating tests carried out at (a) room temperature and (b) 400 °C.

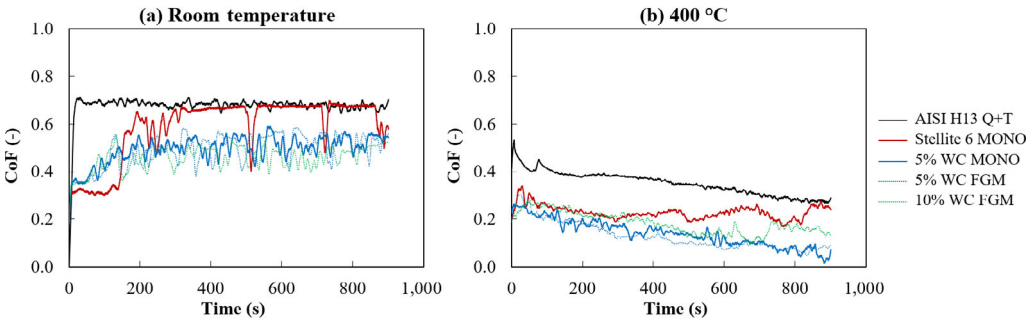

Fig. 14 Friction curves of the reciprocating tests carried out at (a) room temperature and (b) 400 °C.

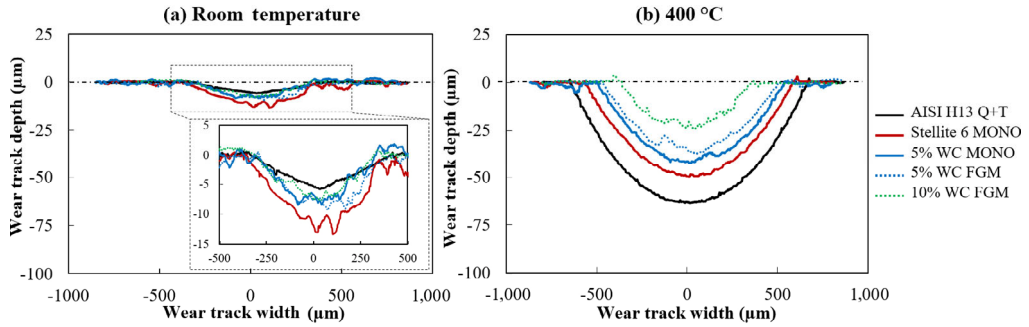

Fig. 15 Cross-sectional profiles of the wear scar for (a) room temperature and (b) 400 °C test specimens.

a higher WC% in the MMC coatings results in higher wear resistance. It must be noted that the lack of surface integrity of the 10% WC FGM specimens did not have an apparent detrimental effect on the tribological behaviour, as the reciprocating tests were carried out in regions with no visible cracks, when possible. In any case, the existing cracks were monitored both before and after tests, and these did not substantially vary in size and no new cracks were formed. As can be observed in Fig. 15, the maximum wear scar depth is 15 µm and 60 µm for RT and high-temperature tests, respectively. Scar depths are well below the thickness of the 4th layer of the coatings (380 µm), indicating that the wear scar was located within the last coating layer. Additionally, 5% WC FGM and mono-composition specimens presented similar results. Thus, it is concluded that the wear resistance of MMC coatings is not affected by the underlying layer, but it is a function of the composition and structure of the top layer and the testing conditions. When comparing RT and 400 °C tests, it is observed that the wear resistance of all samples decreased when tested at 400 °C (see Fig. 15). This can be ascribed to the softening of Stellite alloys at elevated temperatures.

Figure 16 shows the worn surface SEM microphotographs and EDX maps of oxygen corresponding to the 10% WC FGM specimens tested at RT and 400 °C. At room temperature, the SEM microphotograph shows abrasion grooves aligned in the sliding direction (see Fig. 16(a)), indicating a dominant abrasive wear mechanism. Conversely, abrasion grooves were not identified at 400 °C, and the O enrichment on the adhesion zones was observed (see Figs. 16(b)–16(d)), showing that oxidative wear occurred in the friction process. Consequently, a shift in the wear mechanism is observed when increasing the temperature of the wear testing, which is in good accordance with the results reported in Ref. [44].

Adhesive oxides grow slowly on the surface layer and serve as lubricants, decreasing the friction coefficient significantly as compared to the RT tests (see Fig. 13). The hard reinforcement particles, on the other hand, act as load-bearing constituents. Thus, they support the metal matrix and prevent material loss. Note that this is a result of the good bonding between the matrix and reinforcement, as in the present experiment no debonding of the ceramic particles from the matrix during the reciprocating tests has been observed (Figs. 16(a) and 16(b)). In contrast, it

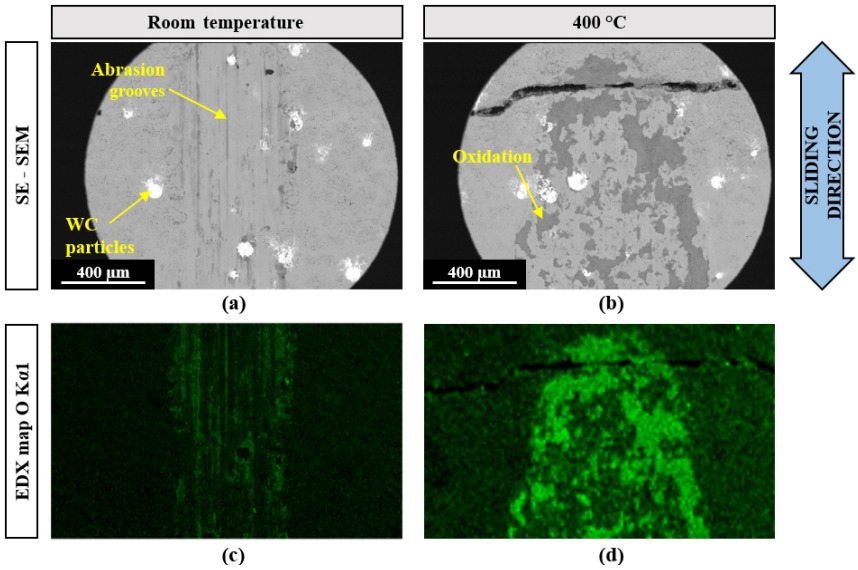

Fig. 16 Worn surface secondary electron SEM microphotographs (a)–(b) and EDX maps of oxygen (c)–(d) of 10% WC FGM specimens tested at RT and 400 °C, respectively.

has been reported in Ref. [44] that ceramic particles often become dislodged from the matrix during sliding wear testing. In those cases, the wear rate of the metal matrix typically increases due to the severe abrasion resulting from the free discrete ceramic particles at the interface between the surface and pin.

Lastly, Fig. 17 shows the axonometric projections of the wear scars measured by optical profilometry. It can be observed that contrary to the RT scars, the scars of the WC-reinforced samples are not homogeneous in shape when tested at 400 °C Figs. 17(c, c1)–17(e, e1).

This phenomenon is associated with the uneven distribution of the ceramic particles, which prevents the matrix from wearing off in the surroundings of such particles. However, this effect is only appearing in the high-temperature wear scars, indicating that the phenomenon is associated with the oxidative wear mechanism and the increased depth of the scar at 400 °C, but does not happen under the abrasive wear mechanism. In Fig. 18, higher magnification axonometric projections and the corresponding images of two heterogeneous regions in sample 10% WC FGM are shown. The inspection of such regions reveals WC particle clusters (clearly visible in Region 2), which result in a reduced depth of the scar in such areas. Indeed, it can be observed that WC particles are worn off at a slower rate and they inhibit the matrix from wearing out in their surroundings. It can be concluded

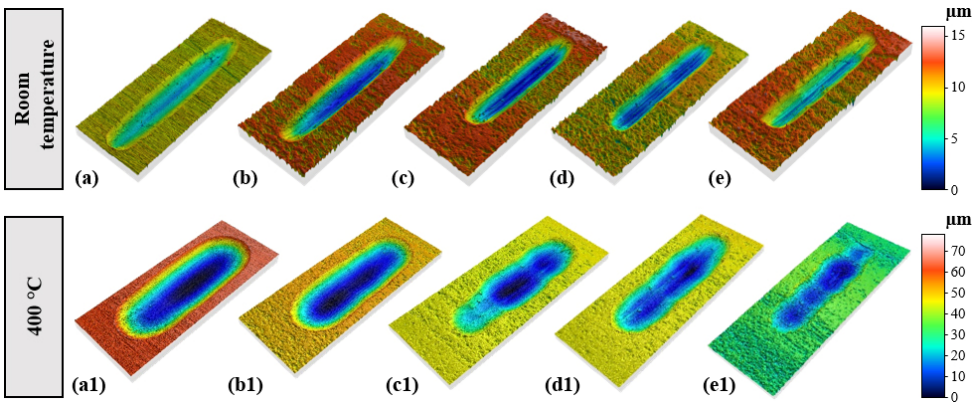

Fig. 17 Axonometric projections of the wear scars measured by optical profilometry of the specimens tested at RT and 400 °C: (a, a1) AISI H13 Q+T, (b, b1) Stellite 6 MONO, (c, c1) 5% WC MONO, (d, d1) 5% WC FGM, and (e, e1) 10% WC FGM. Note the different scales employed to illustrate RT and 400 °C scenarios.

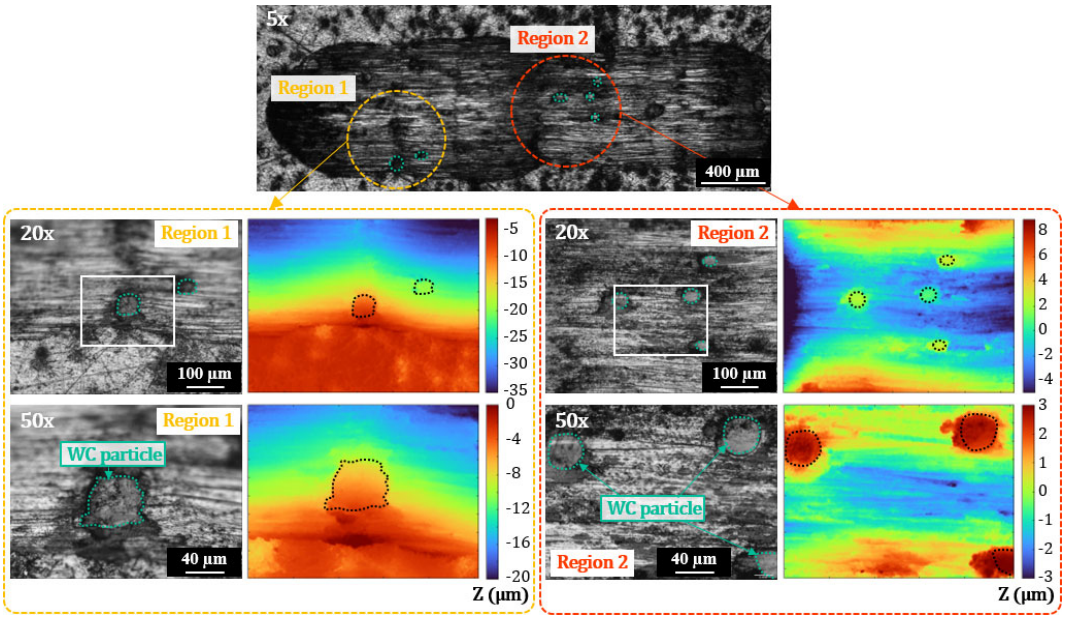

Fig. 18 Details of heterogeneous regions in the scar of a 10% WC FGM sample.

that the random dispersion of the reinforcement particles throughout the surface may cause instabilities and heterogeneous material removal during high-temperature wear testing, but also that they are the reason behind the lower wear rate of ceramic-reinforced MMC coatings. In addition, the faster oxidation at 400 °C and the higher hardness of the WC-reinforced coatings could add up to this phenomenon.

In short, the ability of MMC coatings to protect the surface from high-temperature wear is demonstrated. Furthermore, the wear scar is progressively reduced as the WC% of the coating is increased. Hence, 10% WC coatings exhibit higher wear resistance. In addition, no significant differences in the high-temperature tribological behaviour of FGM and mono-compositional MMC coatings were observed.

4 Conclusions

In the present work, the suitability of L-DED for wear-resistant coating production for die and mould applications has been demonstrated, particularly for high-temperature forming processes. On the one hand, the microstructural aspects of WC-reinforced Stellite 6 coatings have been investigated. On the other hand, the tribological behaviour of such coatings at room temperature and 400 °C has been studied. Lastly, the advantages of employing the FGM strategy for reducing the crack sensitivity of composite materials during the deposition of wear-resistant coatings have been reported. The main contributions of the research work carried out are as follows:

1) The developed processing map for MMC coatings demonstrate that the FGM strategy is an effective tool to prevent surface cracking during the deposition of MMC coatings. Consequently, higher weight fractions of the reinforcement phase are admissible in FGM coatings (5 wt% WC in the present study) as compared to mono-composition coatings (< 5 wt% WC in the present study).

2) As far as the tribological behaviour at room temperature is concerned, the uncoated and heat-treated AISI H13 specimens present a better performance as compared to the coated samples, due to the higher integrity of hot-rolled specimens.

3) In contrast, when tested at 400 °C, coated samples present a significantly better performance as compared to the heat-treated AISI H13 specimens. Besides, the wear resistance is further improved with WC-reinforced coatings. The higher the WC volume fraction, the lower the volume loss and the friction coefficient during the reciprocating testing.

4) The wear mechanism of MMC coatings is dominated by abrasive wear at RT and shifts to oxidative wear at 400 °C. The wear resistance is not affected by the underlying layer, but it is a function

of the composition and structure of the top layer and the testing conditions.

5) WC particles structurally support the metal matrix and reduce material loss. However, the random dispersion and clustering of the WC reinforcement particles throughout the surface cause instabilities and heterogeneous material removal during high-temperature wear testing.

It is concluded that, when an equal composition is ensured at the top layer or the surface coating, a similar performance in terms of tribological behaviour is obtained with FGM and mono-compositional coatings, at least within the scope of the present study. Thus, preliminary results point at the FGM strategy as an interesting approach for L-DED manufacturing of MMCs. The crack sensitivity is reduced, while the tribological behaviour of the coatings remains unaltered. Potentially, a higher WC content can be introduced in FGM samples and, therefore, the wear resistance can be improved to a higher extent.

In the present work, and based on the processing map for L-DED of MMC coatings developed, the implementation of the FGM strategy resulted in an improvement of the wear behaviour at 400 °C of 65% and 54%, for the ECoF and volume loss, for the uncoated specimens; and an improvement of 41% and 26%, for the mono-compositional strategy.

In other words, the FGM strategy enables the fabrication of high-integrity coatings with higher WC content, which ultimately results in better tribological performance at elevated temperatures. Hence, the die and mould industry could benefit from the increased wear resistance and, presumably, lifetime extension of tooling working under high temperatures. However, future work should focus on studying the long-tem operating performance of FGM coatings and also on scaling this technology up to real case studies.

Acknowledgements

This work was supported by the Basque Government (Eusko Jaurlaritza) (Nos. KK-2022/00080 Minaku, KK-2022/00070 Edison) and the Spanish Ministry of Science and Innovation (Nos. PID2019-109220RB-I00 Alasurf, PDC2021-121042-I00 EHU-Coax). The authors would also like to acknowledge the Basque Government (Eusko Jaurlaritza) in call IT 1573-22 for the financial support of the research group.

Declaration of competing interest

The authors have no competing interests to declare that are relevant to the content of this article.

References

[1] European Environmental Agency. Regulation (EU) 2019/631 of the European Parliament and of the Coundcil of 17 April 2019. https://eur-lex.europa.eu/legal-content/EN/ TXT/?uri= CELEX%3A02019R0 631-20210301 (accessed December 2, 2021)

[2] Chantzis D, Liu X C, Politis D J, Shi Z S, Wang L L. Design for additive manufacturing (DfAM) of hot stamping dies with improved cooling performance under cyclic loading conditions. *Addit Manuf* **37**: 101720 (2021)

[3] Bouaziz O, Zurob H, Huang M X. Driving force and logic of development of advanced high strength steels for automotive applications. *Steel Res Int* **84**: 937–947 (2013)

[4] Schirdewahn S, Spranger F, Hilgenberg K, Merklein M. Investigation of the thermal and tribological performance of localized laser dispersed tool surfaces under hot stamping conditions. *Wear* **476**: 203694 (2021)

[5] Neugebauer R, Schieck F, Polster S, Mosel A, Rautenstrauch A, Schönherr J, Pierschel N. Press hardening—An innovative and challenging technology. *Arch Civ Mech Eng* **12**(2): 113–118 (2012)

[6] Batchelor A W, Stachowiak G W. Tribology in materials processing. *J Mater Process Technol* **48**(1–4): 503–515 (1995)

[7] Schwingenschlögl P, Merklein M. Characterization of tribological conditions within direct hot stamping. *J Mater Process Technol* **278**: 116535 (2020)

[8] Emamverdian A A, Sun Y, Cao C P, Pruncu C, Wang Y. Current failure mechanisms and treatment methods of hot forging tools (dies) - a review. *Eng Fail Anal* **129**: 105678 (2021)

[9] Karbasian H, Tekkaya A E. A review on hot stamping. *J Mater Process Technol* **210**(15): 2103–2118 (2010)

[10] Kattire P, Paul S, Singh R, Yan W Y. Experimental characterization of laser cladding of CPM 9V on H13 tool steel for die repair applications. *J Manuf Process* **20**: 492–499 (2015)

[11] Telasang G, Dutta Majumdar J, Padmanabham G, Manna I. Wear and corrosion behavior of laser surface engineered AISI H13 hot working tool steel. *Surf Coat Technol* **261**: 69–78 (2015)

[12] Klocke F, Arntz K, Teli M, Winands K, Wegener M, Oliari S. State-of-the-art laser additive manufacturing for hot-work tool steels. *Procedia CIRP* **63**: 58–63 (2017)

[13] Zeisig J, Schädlich N, Giebeler L, Sander J, Eckert J, Kühn U, Hufenbach J. Microstructure and abrasive wear behavior of a novel FeCrMoVC laser cladding alloy for high-performance tool steels. *Wear* **382–383**: 107–112 (2017)

[14] Wall M T, Pantawane M V, Joshi S, Gantz F, Ley N A, Mayer R, Spires A, Young M L, Dahotre N. Laser-coated CoFeNiCrAlTi high entropy alloy onto a H13 steel die head. *Surf Coat Technol* **387**: 125473 (2020)

[15] Meng Y G, Xu J, Jin Z M, Prakash B, Hu Y Z. A review of recent advances in tribology. *Friction* **8**(2): 221–300 (2020)

[16] Nair A, Ramji V, Durai Raj R, Veeramani R. Laser cladding of Stellite 6 on EN_8 steel—A fuzzy modelling approach. *Mater Today* **39**: 348–353 (2021)

[17] Thawari N, Gullipalli C, Katiyar J K, Gupta T V K. Influence of buffer layer on surface and tribomechanical properties of laser cladded Stellite 6. *Mater Sci Eng B* **263**: 114799 (2021)

[18] Wood P D, Evans H E, Ponton C B. Investigation into the wear behaviour of Stellite 6 during rotation as an unlubricated bearing at 600 °C. *Tribol Int* **44**(12): 1589–1597 (2011)

[19] Weng Z K, Wang A H, Wu X H, Wang Y Y, Yang Z X. Wear resistance of diode laser-clad Ni/WC composite coatings at different temperatures. *Surf Coat Technol* **304**: 283–292 (2016)

[20] Nurminen J, Näkki J, Vuoristo P. Microstructure and properties of hard and wear resistant MMC coatings deposited by laser cladding. *Int J Refract Met Hard Mater* **27**(2): 472–478 (2009)

[21] Bartkowski D, Kinal G. Microstructure and wear resistance of Stellite-6/WC MMC coatings produced by laser cladding using Yb:YAG disk laser. *Int J Refract Met Hard Mater* **58**: 157–164 (2016)

[22] Bartkowski D, Bartkowska A. Wear resistance in the soil of Stellite-6/WC coatings produced using laser cladding method. *Int J Refract Met Hard Mater* **64**: 20–26 (2017)

[23] Li N, Liu W, Wang Y, Zhao Z J, Yan T Q, Zhang G H, Xiong H P. Laser additive manufacturing on metal matrix composites: A review. *Chin J Mech Eng* **34**(1): 1–16 (2021)

[24] Erfanmanesh M, Shoja-Razavi R, Abdollah-Pour H, Mohammadian-Semnani H, Barekat M, Hashemi S H. Friction and wear behavior of laser cladded WC-Co and Ni/WC-Co deposits at high temperature. *Int J Refract Met Hard Mater* **81**: 137–148 (2019)

[25] Wang G Y, Zhang J Z, Shu R Y, Yang S. High temperature wear resistance and thermal fatigue behavior of Stellite-6/WC coatings produced by laser cladding with Co-coated WC powder. *Int J Refract Met Hard Mater* **81**: 63–70 (2019)

[26] Karmakar D P, Muvvala G, Nath A K. High-temperature abrasive wear characteristics of H13 steel modified by laser remelting and cladded with Stellite 6 and Stellite 6/30% WC. *Surf Coat Technol* **422**: 127498 (2021)

[27] Ansari M, Jabari E, Toyserkani E. Opportunities and challenges in additive manufacturing of functionally graded metallic materials via powder-fed laser directed energy deposition: A review. *J Mater Process Technol* **294**: 117117 (2021)

[28] Mostafaei A, Heidarzadeh A, Brabazon D. Production of metal matrix composites via additive manufacturing. *Encycl Mater Compos* **2**: 605–614 (2021)

[29] Xu G J, Kutsuna M, Liu Z J, Sun L Q. Characteristic behaviours of clad layer by a multi-layer laser cladding with powder mixture of Stellite-6 and tungsten carbide. *Surf Coat Technol* **201**(6): 3385–3392 (2006)

[30] Oerlikon Metco. Material Product Data Sheet. Spherical Cast Tungsten Carbide Powder for Laser Cladding, 2023.

[31] Oerlikon Metco. Material Product Data Sheet. Cobalt Chromium [Nickel Tungsten Silicon] Carbon Alloy Products (Similar to Stellite, Ultimet, Mar M 509), 2023.

[32] ASTM International. A681-08(2015) Standard specification for tool steels alloy. ASTM, 2015.

[33] Cillaurren J, Galdos L, Sanchez M, Zabala A, Saenz de Argandoña E, Mendiguren J. Contact pressure and sliding velocity ranges in sheet metal forming simulations. In: Proceedings of *the ESAFORM 2021, 24th International Conference on Material Forming*, Liège, Belgique, 2021.

[34] Hoffmann H, So H, Steinbeiss H. Design of hot stamping tools with cooling system. *CIRP Ann* **56**(1): 269–272 (2007)

[35] Cortina M, Arrizubieta J, Calleja A, Ukar E, Alberdi A. Case study to illustrate the potential of conformal cooling channels for hot stamping dies manufactured using hybrid process of laser metal deposition (LMD) and milling. *Metals* **8**(2): 102 (2018)

[36] ASTM International. ASTM G133-95(2016) Standard test method for linearly reciprocating ball-on-flat sliding wear. ASTM, 2016.

[37] ASTM International. ASTM G203-10(2020) Standard guide for determining friction energy dissipation in reciprocating tribosystems. ASTM, 2020.

[38] Llavori I, Zabala A, Aginagalde A, Tato W, Ayerdi J J, Gómez X. Critical analysis of coefficient of friction derivation methods for fretting under gross slip regime. *Tribol Int* **143**: 105988 (2020)

[39] Ayerdi J J, Aginagalde A, Llavori I, Bonse J, Spaltmann D, Zabala A. Ball-on-flat linear reciprocating tests: Critical assessment of wear volume determination methods and suggested improvements for ASTM D7755 standard. *Wear* **470–471**: 203620 (2021)

[40] Hu Y B, Cong W L. A review on laser deposition-additive manufacturing of ceramics and ceramic reinforced metal matrix composites. *Ceram Int* **44**(17): 20599–20612 (2018)

[41] Xie Z X, Zhang C, Wang R D, Li D, Zhang Y W, Li G S, Lu X G. Microstructure and wear resistance of WC/Co-based coating on copper by plasma cladding. *J Mater Res Technol* **15**: 821–833 (2021)

[42] Farnia A, Ghaini F M, Rao J C, Ocelík V, De Hosson J T M. Tantalum-modified Stellite 6 thick coatings: Microstructure and mechanical performance. *J Mater Sci* **48**(1): 140–149 (2013)

[43] Park S, Park C, Na Y, Kim H S, Kang N. Effects of (W, Cr) carbide on grain refinement and mechanical properties for CoCrFeMnNi high entropy alloys. *J Alloys Compd* **770**: 222–228 (2019)

[44] Alidokht S A, Chromik R R. Sliding wear behavior of cold-sprayed Ni-WC composite coatings: Influence OF WC content. *Wear* **477**: 203792 (2021)

Marta OSTOLAZA. She obtained her M.S. degrees in both Mechanical Engineering (UPV/EHU) and Aerospace Manufacturing (Cranfield University) in 2018. She currently holds a research position at the Department of Mechanical Engineering of the University of the Basque Country (UPV/EHU), while simultaneously working on her Ph.D. Her research work focuses mainly on multi-material additive manufacturing and laser directed energy deposition processes; particularly, on the manufacturing of functionally graded materials and composite materials, for wear resistant coating applications. Her work has resulted in the publication of three indexed scientific articles so far, as well as in several contributions to national and international conferences.